EXCESS HEAT PRODUCTION BY THE ELECTROLYSIS OF AN AQUEOUS POTASSIUM CARBONATE ELECTROLYTE AND THE IMPLICATIONS FOR COLD FUSION

COLD FUSION

TECHNICAL NOTE

KEYWORDS: *cold fusion, calorimetry, electrolysis*

RANDELL L. MILLS *Mills Technologies, The Griest Building Suite 700 I, 8 North Queen Street, Lancaster, Pennsylvania 17603*

STEVEN P. KNEIZYS *Ursinus College, Academic Computing Collegeville, Pennsylvania 19426*

Received February 20, 1991
Accepted for Publication April 1, 1991

According to a novel atomic model, the predominant source of heat of the phenomenon called cold fusion is the electrocatalytically induced reaction whereby hydrogen atoms undergo transitions to quantized energy levels of lower energy than the conventional ground state. These lower energy states correspond to fractional quantum numbers. The hydrogen electronic transition requires the presence of an energy hole of ~27.21 eV provided by electrocatalytic reactants (such as Pd^{2+}/Li^{+}, Ti^{2+}, or K^{+}/K^{+}) and results in "shrunken atoms" analogous to muonic atoms. In the case of deuterium, fusion reactions of shrunken atoms predominantly yielding tritium are possible. Calorimetry of pulsed current and continuous electrolysis of aqueous potassium carbonate (K^{+}/K^{+} electrocatalytic couple) at a nickel cathode is performed in single-cell dewar calorimetry cells. Excess power out exceeded input power by a factor of >37.

I. INTRODUCTION

As a result of the *de facto* assumptions of quantum mechanics and the incomplete or erroneous models that often follow, the prediction and development of useful or functional systems and structures requiring an accurate understanding of atomic structure and energy transfer have been limited. The Schrödinger equation, for example, does not explain the phenomenon referred to as "cold" nuclear fusion: large anomalous heat release and trace tritium production of certain heavy water electrolytic cells having a palladium cathode and a lithium electrolyte. Thus, advances in this field are largely limited to laboratory discoveries that have limited or suboptimal utility. To remedy the shortcomings and inconsistencies of quantum mechanics, Mills and Farrell[1] developed a novel theory for which the fundamental laws of nature are shown to be applicable on all scales. Maxwell's equations, Einstein's general and special relativity, Newtonian mechanics, and the strong and weak forces are unified. Their theory is a quantum theory in which the four quantum numbers of the electron of the one-electron atom arise naturally without gamma factors and provide an explanation for the seemingly contradictory and inconsistent observations of cold fusion. A summary of the development of the theory pertinent to cold fusion follows.

II. THE ONE-ELECTRON ATOM

One-electron atoms include the hydrogen atom, He(I), Li(II), Be(III), and so on. In each case, the nucleus contains Z protons and the atom has a net positive charge of $(Z-1)e$. All forces are central. The mass-energy and angular momentum of the electron are constant; this requires that the equation of motion of the electron be temporally and spatially harmonic. Thus, Laplace's equation applies and

$$\left(\nabla^2 + \frac{1}{v^2}\frac{\delta^2}{\delta t^2}\right) V = 0 \ . \qquad (1)$$

II.A. The Boundary Condition

The condition for radiation by a moving charge is derived from Maxwell's equations. To radiate, the space-time Fourier transform of the charge density function must possess components that are synchronous with waves traveling at the speed of light.[2] Alternatively, for nonradiative states, the charge density function must *not* possess space-time Fourier components that are synchronous with waves traveling at the speed of light.

II.B. The Radial Function

Mills and Farrell[1] do not solve for the radial function from Laplace's equation. Rather, they treat this as a boundary value problem and assume a delta function for the radial function:

$$f(r) = \delta(r - r_n) \ , \qquad (2)$$

where r_n is an allowed radius. [Note that the boundary condition for solution of the radial function of the hydrogen atom with the Schrödinger equation is $\Psi \to 0$ as $r \to 0$. Here, however, the boundary condition is embodied in Eq. (2).] Thus, this trial function implies that the allowed states are two-dimensional spherical shells (zero thickness) of charge density (and mass density) at specific radii r_n. These shells are referred to as electron orbit spheres. When the form of the charge density function is known, the boundary condition (for nonradiation) can be applied to determine specific conditions for r_n. Here, the results of Mills and Farrell[1] are given:

$$2\pi(nr_1) = 2\pi r_n = n\lambda_1 = \lambda_n \ , \tag{3}$$

where

$n = 1,2,3,4,\ldots$

$n = \frac{1}{2},\frac{1}{3},\frac{1}{4},\ldots$

λ_1 = allowed wavelength for $n = 1$

r_1 = allowed radius for $n = 1$.

There are several noteworthy features of Eq. (3):

1. Values of n other than the traditional 1,2,3,..., are allowed.

2. The potential energy is a constant (at a given n) because the electron is at a fixed distance r_n from the nucleus:

$$V_n = \frac{-Ze^2}{4\pi\epsilon_0 r_n} \ , \tag{4}$$

where ϵ_0 is the permittivity of free space.

3. The kinetic energy and velocity squared are constant because the atom does not radiate at r_n and the potential energy is constant:

$$T_n = \tfrac{1}{2}m_e v_n^2 \ . \tag{5}$$

4. The linear momentum must be constant:

$$p_n = \pm m_e v_n \ . \tag{6}$$

5. The wavelength must be constant. Using the de Broglie relationship,

$$\lambda_n = \frac{h}{p_n} = \frac{h}{m_e v_n} \ . \tag{7}$$

II.C. The Angular Function

The radial function for the electron indicates that the electron is two-dimensional. Therefore, the angular mass density function $A(\theta,\phi,t)$ of the electron must be a solution of the Laplace equation in two dimensions (plus time):

$$\left(\nabla^2 + \frac{1}{v^2}\frac{\delta^2}{\delta t^2}\right)A(\theta,\phi,t) = 0 \tag{8}$$

or

$$\left[\frac{1}{r^2\sin\theta}\frac{\delta}{\delta\theta}\left(\sin\theta\frac{\delta}{\delta\theta}\right)_{r\phi} + \frac{1}{r^2\sin^2\theta}\left(\frac{\delta^2}{\delta\phi^2}\right)_{r\theta} + \frac{1}{v^2}\frac{\delta^2}{\delta t^2}\right] \times A(\theta,\phi,t) = 0 \ , \tag{9}$$

where v is the linear velocity of the electron.

Conservation of momentum and energy allows the angular functions and time functions to be separated:

$$A(\theta,\phi,t) = Y(\theta,\phi)K(t) \ . \tag{10}$$

Charge is conserved as well, and the charge of an electron can be superimposed on its mass. That is, the angular mass density function $A(\theta,\phi,t)$ is also the angular charge density function.

The electron orbit sphere experiences a constant potential energy because it is fixed at $r = r_n$. To avoid being pulled into the nucleus, the orbit sphere must rotate. It is the rotation of the orbit sphere that causes angular momentum. The rotational energy of a rotating body is

$$E_{rotational} = \tfrac{1}{2}I\omega^2 \ , \tag{11}$$

where

I = moment of inertia

ω = angular velocity.

The angular velocity must be constant (at a given n) because r is constant, and the energy and angular momentum are constant. The allowed angular velocities are related to the allowed frequencies by

$$\omega_n = 2\pi\nu_n \ . \tag{12}$$

The allowed frequencies are related to the allowed velocities by

$$v_n = \nu_n\lambda_n \ . \tag{13}$$

The allowed velocities and angular frequencies are related to r_n by

$$v_n = r_n\omega_n \ , \tag{14}$$

$$\omega_n = \frac{\hbar}{m_e r_n^2} \ , \tag{15}$$

and

$$v_n = \frac{\hbar}{m_e r_n} \ . \tag{16}$$

The magnitude of the angular momentum $|L|$ must be constant. The constant is $\hbar$:

$$|L_n| = m_e v_n r_n = m_e\frac{\hbar}{m_e r_n}r_n = \hbar \ . \tag{17}$$

Thus, Eq. (9) becomes

$$-\frac{\hbar^2}{2I}\left[\frac{1}{\sin\theta}\frac{\delta}{\delta\theta}\left(\sin\theta\frac{\delta}{\delta\theta}\right)_{r\phi} + \frac{1}{\sin^2\theta}\left(\frac{\delta^2}{\delta\phi^2}\right)_{r\theta}\right] \times A(\theta,\phi,t) = EA(\theta,\phi,t) \ . \tag{18}$$

The space-time angular function $A(\theta,\phi,t)$ is separated into an angular function and a time function, $Y(\theta,\phi)K(t)$. The time-harmonic function $K(t) = \exp(i\omega_n t)$ is a solution. [Here, again, the boundary condition (for nonradiation) determines the specific conditions for ω_n.] When the time-harmonic function is eliminated,

$$-\frac{\hbar^2}{2I}\left[\frac{1}{\sin\theta}\frac{\delta}{\delta\theta}\left(\sin\theta\frac{\delta}{\delta\theta}\right)_{r\phi} + \frac{1}{\sin^2\theta}\left(\frac{\delta^2}{\delta\phi^2}\right)_{r\theta}\right] \times Y(\theta,\phi) = EY(\theta,\phi) \ . \tag{19}$$

Equation (19) is the equation for the rigid rotor. The angular function can be separated into a function of Θ and a function of Φ, and the solutions are well known.[3] The energies are given by

$$E_{rotational} = \frac{\hbar^2 l(l+1)}{2I} \ , \quad l = 0,1,2,3,\ldots \ . \tag{20}$$

The angular functions are the spherical harmonics $Y_l^m(\phi,\theta)$. The spherical harmonic $Y_s(\phi,\theta) = 1$, $s = \frac{1}{2}$, is also a solution. The spherical harmonics can be positive or negative (depending on θ); the most negative value is -1. But the mass of the electron cannot be negative, and the charge cannot be positive. Thus, to ensure that the function is always positive or zero, the form of the angular solution must be

$$Y_S(\phi,\theta) + Y_l^m(\phi,\theta) \ , \tag{21}$$

where $Y_S(\phi,\theta)$ is called the angular spin function and $Y_l^m(\phi,\theta)$ is called the angular orbital function. The function $Y_l^m(\phi,\theta)$ can be thought of as a modulation function. Thus, the angular momentum can be thought of as arising from a spin component and an orbital component that have corresponding energies. One result of this model for $l = 0$ [uniform charge (mass) density] is that some of the angular momentum (kinetic energy) is not counted in the spin angular momentum (rotational energy). That is, for any spin axis, there is an infinite number of great circles with planes passing through that axis with angles other than 90 deg. All points on any one of these great circles are moving, but not all of that motion is part of the spin angular momentum (rotational energy); only that motion perpendicular to the spin axis is part of the spin angular momentum (rotational energy). Thus, the spin angular momentum (rotational energy) is always less than the total angular momentum (kinetic energy). The following relationships must hold:

$$E_{rotational} = \tfrac{1}{2}I\omega^2 \le \tfrac{1}{2}mv^2 \ , \tag{22}$$

$$I\omega \le \hbar \ , \tag{23}$$

and

$$I \le mr^2 \ . \tag{24}$$

Furthermore, it is known from the Stern-Gerlach experiment that a beam of silver atoms splits into two components when passed through an inhomogeneous magnetic field. The measured spin angular momentum is $\sqrt{\frac{3}{4}}\hbar$, and the angular momentum in the direction of the applied field is $\pm\hbar/2$. Given a uniform density of points traveling on great circles with a total angular momentum of $\hbar$, it can be shown[1] that the projection of the total angular momentum onto the spin axis is $\sqrt{\frac{3}{4}}\hbar$. The Stern-Gerlach experiment implies a magnetic moment of one Bohr magneton and an associated angular momentum quantum number of $\frac{1}{2}$. Historically, this quantum number is called the spin quantum number m_s, and that designation is maintained.

II.D. The Magnetic Field from the Spinning Orbit Sphere

The orbit sphere is a spinning shell of negative charge. For $l = 0$, the orbit sphere gives rise to a magnetic moment of one Bohr magneton,[3]

$$\beta = \frac{e\hbar}{2m_e} = 9.274 \times 10^{-24} \text{ J/T} \ , \tag{25}$$

and a magnetic field,[1]

$$H = \begin{cases} \dfrac{e\hbar}{m_e r_n^3}\left(\hat{i}_r \cos\theta - \hat{i}_\theta \sin\theta\right) \ , & \text{for } r < r_n \quad (26) \\ \dfrac{e\hbar}{2m_e r^3}\left(\hat{i}_r 2\cos\theta - \hat{i}_\theta \sin\theta\right) \ , & \text{for } r > r_n \ . \quad (27) \end{cases}$$

Note that the magnetic field is a constant for $r < r_n$.

It can be shown[1] that the energy stored in the magnetic field of the electron orbit sphere is

$$E_{mag} = \frac{\pi\mu_0 e^2\hbar^2}{m_e^2 r_n^3} \ . \tag{28}$$

II.E. Determination of r_n

The one-electron orbit sphere is a spherical shell of negative charge (total charge $= -e$) of zero thickness at a distance r_n from the nucleus (charge $= +Ze$). For the ground state ($n = 1$), the centrifugal force of the electron is given by

$$f_{centrifugal} = \frac{m_e v_1^2}{r_1} \ . \tag{29}$$

The centripetal force is the Coulombic force f_{Coul} between the electron and the nucleus:

$$f_{Coul} = \frac{Z_{eff}e^2}{4\pi\epsilon_0 r_1^2} \ , \tag{30}$$

where ϵ_0 is the permittivity of free space. Thus,

$$\frac{m_e v_1^2}{r_1} = \frac{Ze^2}{4\pi\epsilon_0 r_1^2} \ . \tag{31}$$

Using Eq. (16),

$$r_1 = \frac{4\pi\epsilon_0\hbar^2}{Ze^2 m_e} \ . \tag{32}$$

The Bohr radius is substituted into Eq. (32):

$$a_0 = \frac{4\pi\epsilon_0\hbar^2}{e^2 m_e} \tag{33}$$

and

$$r_1 = \frac{a_0}{Z} \ . \tag{34}$$

II.F. Energy Calculations

The potential energy V can be calculated from the force between the electron and the nucleus [Eq. (30)] and the radius r_1:

$$V = \frac{-Ze^2}{4\pi\epsilon_0 r_1} = \frac{-Z^2e^2}{4\pi\epsilon_0 a_0} = -Z^2 \times 4.3675 \times 10^{-18} \text{ J}$$
$$= -Z^2 \times 27.2 \text{ eV} \ . \tag{35}$$

Because this is a central force problem, the kinetic energy T is $-\frac{1}{2}V$:

$$T = \frac{Z^2e^2}{8\pi\epsilon_0 a_0} = Z^2 \times 13.159 \text{ eV} \ . \tag{36}$$

The same result can be obtained from $T = \frac{1}{2}m_e v_1^2$ and Eq. (16).

Alternatively, the kinetic energy, which is equal to the stored electric energy E_{elec}, can be calculated from[4]

$$T = E_{elec} = -\frac{1}{2}\epsilon_0 \int_\infty^{r_1} \epsilon^2 \, dv \ , \tag{37}$$

where

$$\epsilon = \frac{Ze}{4\pi\epsilon_0 r^2} \ .$$

Thus, as the orbit sphere shrinks from ∞ to r_1,

$$E_{ele} = -\frac{1}{2}\epsilon_0 \int_0^{2\pi}\int_0^{\pi}\int_{\infty}^{r_1} \epsilon^2 r^2 \sin\theta \, dr \, d\theta \, d\Phi \quad (38)$$

$$= -\frac{Z^2e^2}{8\pi\epsilon_0}\int_{\infty}^{r_1}\frac{1}{r^2}\,dr \quad (39)$$

$$= \frac{Z^2e^2}{8\pi\epsilon_0 a_0} = Z^2 \times 2.1837 \times 10^{-18} \text{ J}$$

$$= Z^2 \times 13.589 \text{ eV} . \quad (40)$$

III. EXCITED STATES OF THE ONE-ELECTRON ATOM

It is well known that resonator cavities can trap electromagnetic radiation of discrete resonant frequencies. The orbit sphere is a resonator cavity and can trap photons of discrete frequencies. Thus, photon absorption occurs as an excitation of a resonator mode.

An electron in the ground state ($n = 1$) is in force balance:

$$\frac{m_e v_1^2}{r_1} = \frac{Ze^2}{4\pi\epsilon_0 r_1^2} . \quad (41)$$

When an electron in the ground state absorbs a photon of sufficient energy to take it to a new nonradiative state ($n = 2,3,4,\ldots$), force balance must be maintained. This is possible only if $Z_{eff} = Z/n$; therefore,

$$\frac{m_e v_n^2}{r_n} = \frac{Z_{eff}e^2}{4\pi\epsilon_0 r_n^2} . \quad (42)$$

The reduction of the charge from Ze to Ze/n is caused by trapping a photon in the orbit sphere cavity—a spherical cavity. The photon's electric field creates standing waves in the cavity with an effective charge of $(-1 + 1/n)Ze$ (at r_n). The total charge experienced by the electron is the sum of the proton and photon charge components. The equation for these trapped photons can be solved as a boundary value problem of Laplace's equation.

For the hydrogen atom, the boundary conditions are that the radial electric field of the photon at r_n is

$$\epsilon \hat{i}_{r\,photon} = \left(-1 + \frac{1}{n}\right)\frac{e}{4\pi\epsilon_0 (r_n)^2} , \quad n = 2,3,4,\ldots, . \quad (43)$$

The general form of the solution to Laplace's equation in spherical coordinates is

$$\Phi(r,\theta,\phi) = \sum_{l=0}^{\infty}\sum_{m=-l}^{l}[A_{l,m}r^l + B_{l,m}r^{-(l+1)}] \times [Y_{l,m}(\theta,\phi) + Y_s(\theta,\phi)] . \quad (44)$$

All $A_{l,m}$ are zero because the electric field given by the potential must be inversely proportional to the radius to obtain force balance. The electric field is the gradient of the potential:

$$\epsilon = -\nabla\Phi \quad (45)$$

and

$$\epsilon \hat{i}_r = -\frac{\delta\Phi}{\delta r}\hat{i}_r . \quad (46)$$

Thus,

$$\epsilon \hat{i}_r = \sum_{l=0}^{\infty}\sum_{m=-l}^{l} B_{l,m}(l+1)r^{-(l+2)}[Y_l^m(\phi,\theta) + Y_S^{m_s}(\phi,\theta)] . \quad (47)$$

Given that $\epsilon(proton) = +e/4\pi\epsilon_0 r_n^2$ and that the electric fields of the proton and photon must superimpose to yield a field equivalent to a central point charge of $+Ze/n$, the photon electric field for each mode is determined as follows. The angular part of the charge density function of the orbit sphere at force balance must be in phase with the electric field of the orbit sphere because the relationship between the total electric field equation and the photon charge density function is given by Maxwell's equation in two dimensions:

$$n\cdot(\epsilon_1 - \epsilon_2) = \frac{\sigma}{\epsilon_0} , \quad (48)$$

where

n = normal unit vector ($\hat{i}_r$)

$\epsilon_1 = 0$ = electric field outside of the orbit sphere

ϵ_2 = total electric field at $r_n = na_0$

σ = surface charge density.

Thus,

$$\epsilon \hat{i}_{r\,photon}|_{r_n = na_0} = \frac{e^2}{4\pi\epsilon_0 (na_0)^2}\left(-1 + \frac{1}{n}\,\text{Re}\{i[Y_l^m(\phi,\theta) + Y_S^{m_s}(\phi,\theta)]\}\right) \quad (49)$$

$$= \sum_{l=0}^{\infty}\sum_{m=-l}^{l} -B_{l,m}(l+1)(na_0)^{-(l+2)} \times \text{Re}\{i[Y_l^m(\phi,\theta) + Y_s^{m_s}(\phi,\theta)]\} , \quad (50)$$

for

$$n = 2,3,4,\ldots$$

$$l = 1,2,\ldots,n-1$$

$$m = -l,-l+1,\ldots,0,\ldots,+l ,$$

and

$$\epsilon \hat{i}_{r\,photon\,n,l,m}|_{r_n = na_0} = \frac{e^2}{4\pi\epsilon_0 (na_0)^2}\left(-1 + \frac{1}{n}\,\text{Re}\{i[Y_l^m(\phi,\theta) + Y_S^{m_s}(\phi,\theta)]\}\right) . \quad (51)$$

Therefore,

$$\sum_{l=0}^{\infty}\sum_{m=-l}^{l} B_{l,m} = \frac{e(na_0)^l}{4\pi\epsilon_0 (l+1)}\left(-1 + \frac{1}{n}\right) \quad (52)$$

and

$$\epsilon \hat{i}_{r\,photon\,n,l,m} = \frac{e(na_0)^l}{4\pi\epsilon_0}\frac{1}{r^{(l+2)}} \times \left(-1 + \frac{1}{n}\,\text{Re}\{i[Y_l^m(\phi,\theta) + Y_S^{m_s}(\phi,\theta)]\}\right) , \quad (53)$$

where

$\epsilon\hat{i}_{r\,total}$ = sum of the photon and proton electric fields:

$$\epsilon\hat{i}_{r\,total} = \frac{e}{4\pi\epsilon_0 r^2} + \frac{e(na_0)^l}{4\pi\epsilon_0}\frac{1}{r^{(l+2)}} \times \left(-1 + \frac{1}{n}\,\mathrm{Re}\{i[Y_l^m(\phi,\theta) + Y_s^{m_s}(\phi,\theta)]\}\right) . \quad (54)$$

For $r = na_0$, the magnitude of the total radial electric field is

$$\epsilon\hat{i}_{r\,total} = \left[\frac{e}{4\pi\epsilon_0(na_0)^2} + \frac{e}{4\pi\epsilon_0(na_0)^2}\right]\left(-1 + \frac{1}{n}\right) \quad (55)$$

and

$$\epsilon\hat{i}_{r\,total} = \frac{1}{n}\frac{e}{4\pi\epsilon_0(na_0)^2} . \quad (56)$$

For quantum numbers n, l, and m, the potential functions are solutions to Laplace's equation. All boundary conditions are met for the corresponding electric fields. Thus, Eq. (54) is the solution of the excited modes of the resonator cavity (orbit sphere). And, the quantum numbers of the electron are n, l, $m(m_l)$, and m_s, as described in Sec. II.

The energy of the photon that excites a mode in a stationary spherical resonator cavity from radius a_0 to radius na_0 is

$$E_{photon} = \frac{e^2}{4\pi\epsilon_0 a_0}\left(1 - \frac{1}{n^2}\right) = h\nu = \hbar\omega . \quad (57)$$

After multiplying Eq. (57) by

$$\frac{a_0}{a_0} = \frac{4\pi\epsilon_0\hbar^2}{e^2 m_e a_0} ,$$

where a_0 is given by Eq. (33), ω_{photon} is

$$\omega_{photon} = \frac{\hbar}{m_e a_0^2}\left(1 - \frac{1}{n^2}\right) . \quad (58)$$

In the case of an electron orbit sphere, the resonator possesses kinetic energy before and after the excitation. The kinetic energy is always one-half of the potential energy. As a result, the energy and angular frequency to excite an electron orbit sphere is only one-half of the values in Eqs. (57) and (58).

The angular velocity of an electron orbit sphere of radius na_0 is

$$\omega_n = \frac{\hbar}{m_e(na_0)^2} . \quad (59)$$

The change in angular velocity of the orbit sphere for an excitation from $n = 1$ to $n = n$ is

$$\Delta\omega = \frac{\hbar}{m_e(a_0)^2} - \frac{\hbar}{m_e(na_0)^2} = \frac{\hbar}{m_e(a_0)^2}\left(1 - \frac{1}{n^2}\right) . \quad (60)$$

The kinetic energy change of the transition is

$$\frac{1}{2}m_e(\Delta v)^2 = \frac{1}{2}\frac{e^2}{4\pi\epsilon_0 a_0}\left(1 - \frac{1}{n^2}\right) = \frac{1}{2}\hbar\omega . \quad (61)$$

The change in angular velocity of the electron orbit sphere [Eq. (60)] is identical to the angular velocity of the photon necessary for the excitation ω_{photon} [Eq. (58)]. The energy of the photon to excite the equivalent transition in an electron orbit sphere is one-half of the excitation energy of the stationary cavity because the change in kinetic energy of the electron orbit sphere supplies one-half of the necessary energy. The photon can carry zero or $\pm\hbar$ units of angular momentum [Eq. (17)]. Thus, during excitation, the spin, orbital, or total angular momentum of the orbit sphere can change by zero or $\pm\hbar$. The electron transition rules arise from conservation of angular momentum. The radius of an orbit sphere increases with the absorption of electromagnetic energy. On ionization, the orbit sphere radius goes to infinity, and the electron is a plane wave (consistent with double-slit experiments) with a de Broglie wavelength of $\lambda = h/p$.

IV. PAIR PRODUCTION

Matter and energy are interconvertible and are, in essence, different states of the same entity. The state, matter or energy, is determined by the laws of nature and the properties of space-time. A photon propagates according to Maxwell's equations at the speed of light in space-time with intrinsic impedance η. Matter as a fundamental particle is created in space-time from a photon. Matter obeys the laws of special relativity, the relationship of motion to space-time, and space-time is curved by matter according to the laws of general relativity. Relationships must exist between these laws and the implicit fundamental constants. The conversion of energy into matter requires a transition state in which the identification of the entity as matter or energy is impossible. From the properties of the entity, as matter or energy, and from the physical laws and the properties of space-time, the transition state hereafter called a virtual orbit sphere is derived.

For example, a photon of energy 1.02 MeV becomes a positron and an electron in the presence of charge. This phenomenon, called pair production, involves the conservation of mass/energy, charge, and angular momentum. Pair production occurs as an event in space-time where all boundary conditions are met according to the physical laws: Maxwell's equations, Newton's laws, and Einstein's special and general relativity, where matter and energy are indistinguishable by any physical property. Matter exists as orbit spheres; thus, the conversion of energy to matter must involve the orbit sphere equations derived earlier. It must also depend on the equations of electromagnetic radiation and the properties of space-time because matter is created from electromagnetic radiation as an event in space-time.

Matter and light obey the wave equation relationship:

$$v = \lambda\frac{\omega}{2\pi} . \quad (62)$$

The boundary condition for nonradiation by a virtual orbit sphere is

$$2\pi(r_n^*) = 2\pi(nr_1^*) = n\lambda_1^* = \lambda_n^* , \quad (63)$$

where

$$n = 1,2,3,4,\ldots$$

or

$$n = \tfrac{1}{2},\tfrac{1}{3},\tfrac{1}{4},\ldots ,$$

and where r^* and λ^* are the allowed radii and wavelengths for the virtual matter in question.

The relationship between the potential energy of an

electron orbit sphere and the angular velocity of the orbit sphere is

$$V = \hbar\omega^* = \frac{1}{n}\frac{e^2}{4\pi\epsilon_0 n a_0} . \quad (64)$$

It can be demonstrated that the velocity of the electron orbit sphere satisfies the relationship for the velocity of a wave by substitution of Eqs. (3) and (15) into Eq. (62), which gives Eq. (16). Similarly, the relationship among the velocity of light in free space c, frequency ω, and wavelength λ is

$$c = \lambda\frac{\omega}{2\pi} , \quad (65)$$

and the energy of a photon of frequency ω is

$$E = \hbar\omega . \quad (66)$$

Recall from Sec. III that a photon of discrete frequency ω can be trapped in the orbit sphere of an electron that serves as a resonator cavity of radius r_n where the resonance excitation energy of the cavity is given by Eq. (64).

The angular velocities of the orbit sphere and trapped photon are the same, and the ratio of their linear velocities is

$$\frac{v_n}{c_{photon}} = \frac{\lambda_n\frac{\omega_n}{2\pi}}{\lambda_{photon}\frac{\omega_{photon}}{2\pi}} = \frac{\lambda_n}{\lambda_{photon}} , \quad (67)$$

where the subscripts n refer to orbit sphere quantities.

Consider a virtual electron orbit sphere, which is defined as the transition state between light and matter where light and matter are indistinguishable. For this case, the velocity of the electron virtual orbit sphere is the speed of light in the inertial reference frame of the photon that formed the virtual orbit sphere. Substituting c for v_n in Eq. (62), λ_n given by Eq. (3) [where r_1 is given by Eqs. (32) and (33)] for λ, and of ω_n given by Eq. (15) for ω results in

$$c = 2\pi n a_0\frac{\hbar}{m_e(na_0)^2} . \quad (68)$$

Maxwell's equations provide that

$$c = \left(\frac{1}{\epsilon_0\mu_0}\right)^{1/2} . \quad (69)$$

The result of substituting Eqs. (33) and (69) into Eq. (68) is

$$\frac{1}{n} = \frac{\hbar}{m_e c a_0} = \frac{\hbar(\epsilon_0\mu_0)^{1/2}}{m_e}\frac{e^2 m_e}{4\pi\epsilon_0\hbar^2} = \frac{1}{4\pi}\left(\frac{\mu_0}{\epsilon_0}\right)^{1/2}\frac{e^2}{\hbar} = \alpha^{-1} . \quad (70)$$

In fact, α is the fine-structure constant (a dimensionless constant for pair production).[5] The experimental value is $\frac{1}{137.03604}$. However, by the boundary condition for nonradiation [Eqs. (3) and (63)] $1/n$ must be 1 divided by an integer. That integer is exactly 137.

The permeability μ_0 of free space is defined as $4\pi \times 10^{-7}$ N/A^{-2}. The experimental permittivity ϵ_0 of free space is extremely close to $1/36\pi \times 10^{-9}$ F/m, and the experimental value of $e^2/\hbar$ is extremely close to $\frac{1}{4110}$.

To match the boundary condition [Eq. (3)], $\hbar/e^2 = 4110 = (30)(137)$ exactly, and $\epsilon_0 = 1/36\pi \times 10^{-9}$ F/m exactly.

In a similar fashion, the intrinsic impedance of free space can be calculated as

$$\eta = \left(\frac{\mu_0}{\epsilon_0}\right)^{1/2} = \left(\frac{4\pi \times 10^{-7}}{\frac{1}{36\pi} \times 10^{-9}}\right)^{1/2} = 120\pi\Omega , \quad (71)$$

and the speed of light is determined to be exactly

$$c = \frac{1}{(\mu_0\epsilon_0)^{1/2}} = 3 \times 10^8 \text{ m/s} . \quad (72)$$

The result that c is exactly 3×10^8 m/s may appear counterintuitive given the arbitrary nature of the definitions of metres and seconds. However, mks units are not arbitrary. They are defined according to mutually dependent relationships between the constants and the electric and magnetic force laws. The units take on significance by the definition of μ_0 in terms of Newtons per square ampere. It can be demonstrated[1] that this definition fixes the exact value of the constants and gives rise to an exact definition of the second, metre, and kilogram.

The radius of the virtual electron orbit sphere is $a_0/137$, and the potential energy V is given by Eq. (64), where n is $\frac{1}{137}$:

$$V = -\frac{(137)^2 e^2}{4\pi\epsilon_0 a_0} . \quad (73)$$

Substituting

$$a_0 = \frac{4\pi\epsilon_0\hbar^2}{m_e e^2} ,$$

$$\frac{\hbar}{e^2} = (30)(137) ,$$

$$\eta = \left(\frac{\mu_0}{\epsilon_0}\right)^{1/2} = 120\pi ,$$

and

$$c = \left(\frac{1}{\epsilon_0\mu_0}\right)^{1/2}$$

into Eq. (73) results in

$$V = m_e c^2 . \quad (74)$$

Furthermore, the result of the multiplication of both sides of Eq. (15) by $\hbar$, $r_n = na_0$, and substituting

$$n = \tfrac{1}{137} ,$$

$$a_0 = \frac{4\pi\epsilon_0\hbar^2}{m_e e^2} ,$$

$$\frac{\hbar}{e^2} = (30)(137) ,$$

$$\eta = \left(\frac{\mu_0}{\epsilon_0}\right)^{1/2} = 120\pi ,$$

and

$$c = \left(\frac{1}{\epsilon_0\mu_0}\right)^{1/2}$$

yields

$$\hbar\omega^*_{1/137} = m_e c^2 . \quad (75)$$

The relativistic factor,

$$\gamma = \frac{1}{\left[1 - \left(\frac{v}{c}\right)^2\right]^{1/2}} ,$$

for an orbit sphere at radius $r^*/137$ ($a_0/137$ for the electron) is 2π. The energy stored in the magnetic field of the electron orbit sphere is

$$E_{mag} = \frac{\pi \mu_0 e^2 \hbar^2}{(m_e)^2 r_n^3} . \quad (76)$$

As a result of substituting $a_0/137$ for r_n, 137 for Z_{eff} (recall that $r_n = a_0/Z_{eff}$), the relativistic mass $2\pi m_e$ for m_e,

$$a_0 = \frac{4\pi\epsilon_0\hbar^2}{m_e e^2} ,$$

$$\frac{\hbar}{e^2} = (30)(137) ,$$

$$\eta = \left(\frac{\mu_0}{\epsilon_0}\right)^{1/2} = 120\pi ,$$

and

$$c = \left(\frac{1}{\epsilon_0\mu_0}\right)^{1/2}$$

is

$$E_{mag} = m_e c^2 . \quad (77)$$

Thus, the energy stored in the magnetic field of the virtual electron orbit sphere equals the electrical potential energy of the virtual orbit sphere. The magnetic field is a relativistic effect of the electrical field; thus, equivalence of the potential and magnetic energies when $v = c$ is given by special relativity where these energies are calculated using Maxwell's equations. The energy stored in the electric and magnetic fields of a photon are equivalent. The corresponding equivalent energies of the virtual orbit sphere are the electrical potential energy and the energy stored in the magnetic field of the orbit sphere.

Space-time is an electrical LC circuit with an intrinsic impedance of exactly

$$\eta = \left(\frac{\mu_0}{\epsilon_0}\right)^{1/2} = \left(\frac{4\pi \times 10^{-7}}{\frac{1}{36\pi} \times 10^{-9}}\right)^{1/2} = 120\pi . \quad (78)$$

The circumference of the virtual electron orbit sphere is $2\pi a_0/137$. The relativistic factor for the radius of $a_0/137$ is 2π; thus, due to relativistic length contraction, the total capacitance of free space of the virtual orbit sphere of radius $a_0/137$ is

$$C = \frac{2\pi \frac{a_0}{137} \epsilon_0}{2\pi} = \epsilon_0 \frac{a_0}{137} , \quad (79)$$

where ϵ_0 is the capacitance of space-time per unit length (farad per metre). Similarly, the inductance is

$$L = \frac{2\pi \frac{a_0}{137} \mu_0}{2\pi} = \mu_0 \frac{a_0}{137} , \quad (80)$$

where μ_0 is the inductance per unit length (henry per metre).

Thus, the resonance frequency of a virtual electron orbit sphere is

$$\omega^* = \frac{1}{(LC)^{1/2}} = \frac{1}{\left(\epsilon_0 \frac{a_0}{137} \mu_0 \frac{a_0}{137}\right)^{1/2}} . \quad (81)$$

Using

$$a_0 = \frac{4\pi\epsilon_0\hbar^2}{m_e e^2} ,$$

$$\frac{\hbar}{e^2} = (30)(137) ,$$

$$\eta = \left(\frac{\mu_0}{\epsilon_0}\right)^{1/2} = 120\pi ,$$

and

$$c = \left(\frac{1}{\epsilon_0\mu_0}\right)^{1/2} ,$$

then

$$\omega^* = \frac{m_e c^2}{\hbar} . \quad (82)$$

Thus, the LC resonance frequency of free space for a virtual electron orbit sphere equals the angular frequency of the photon that forms the virtual orbit sphere.

The impedance of any LC circuit goes to infinity when it is excited at the resonance frequency. Thus, the electron virtual orbit sphere is an LC circuit excited at the corresponding resonance frequency of free space. The impedance of free space becomes infinite, and electromagnetic radiation cannot propagate. At this event, the frequency, wavelength, velocity, and energy of the virtual orbit sphere are equal to that of the photon. The mass/energy of the electron virtual orbit sphere is exactly the rest mass at infinity. Thus, a real orbit sphere electron is formed at infinity (with zero velocity) from the electron virtual orbit sphere in the presence of a central electric field of

$$\epsilon = \frac{+e}{4\pi\epsilon_0 r^2} , \quad (83)$$

where all of the electron virtual orbit sphere equations developed herein apply to this central field.

Actually, due to conservation of charge, a positron and an electron are formed of two photons of energy equal to the rest mass/energy of the electron. (Photons superimpose; thus, pair production occurs with a single photon of energy equal to twice the rest mass of an electron.)

For pair production, angular momentum is conserved. All photons carry $\hbar$ angular momentum, and the angular momentum of all matter as orbit spheres is $\hbar$ [see Eq. (17)]. The radius of particle creation is $r_1^*/137$. This radius is equal to the Compton wavelength bar λ_c, where $\lambda_c = \hbar/mc$. It arises naturally from the boundary condition of no radiation [Eqs. (3) and (63)], (where $n = \frac{1}{137}$), the de Broglie relationship [Eq. (7)], and the fact that the velocity of the virtual orbit sphere equals c:

$$r_{1/137}^* = \frac{\hbar}{mc} = \lambda_c . \quad (84)$$

The correct prediction of electron and positron creation (pair production) having a dimensionless cross section of $\frac{1}{137}$ establishes the validity of electron states corresponding to fractional quantum numbers. In Sec. V, it is demonstrated that

the transition to fractional quantum states and the resulting "shrunken" atoms account for the phenomenon called cold fusion.

V. HECTER AND COULOMBIC ANNIHILATION FUSION (COLD FUSION)

For the hydrogen atom, the radius of the ground-state orbit sphere is a_0. This orbit sphere contains no photonic waves, and the centripetal force and the Coulombic force balance. Thus,

$$\frac{m_e v_1^2}{a_0} = \frac{e^2}{4\pi\epsilon_0 a_0^2} . \quad (85)$$

It is shown in Sec. III that the electron orbit sphere is a resonator cavity that can trap electromagnetic radiation of discrete frequencies. The photon potential functions are solutions of Laplace's equation. The photons decrease the nuclear charge to $1/n$ and increase the radius of the orbit sphere to na_0. The new configuration is also in force balance:

$$\frac{m_e v_n^2}{na_0} = \frac{e^2/n}{4\pi\epsilon_0 (na_0)^2} . \quad (86)$$

Mills and Farrell[1] propose, however, that the orbit sphere resonator can trap photons that increase the nuclear charge and decrease the radius of the orbit sphere. This occurs, for example, when the orbit sphere couples to another resonator cavity that can absorb energy—this is the absorption of an energy hole. The absorption of an energy hole destroys the balance between the centrifugal force and the increased central Coulombic force. As a result, the electron is pulled toward the nucleus. If another allowed state that obeys the boundary conditions is not available, the electron plunges into the nucleus.

Now, recall that, for the He^+ ion ($Z = 2$, a one-electron atom), an allowed state exists at $0.5a_0$. It can be shown that if a ground-state hydrogen atom emits a photon of ~27 eV, two photons are created—one is ejected and one remains in the orbit sphere. The photonic wave in the orbit sphere creates an effective charge at the orbit sphere such that the electron experiences an effective charge of $+2e$ and establishes a new centripetal/Coulombic equilibrium at $r_{1/2} = 0.5a_0$. That is, the orbit sphere shrinks from $r_1 = a_0$ to $r_{1/2} = a_0/2$:

$$V = -\frac{Z_{eff} e^2}{4\pi\epsilon_0 r_{1/2}} = -\frac{2 \times 2e^2}{4\pi\epsilon_0 a_0}$$

$$= -4 \times 27.178 \text{ eV} = -108.70 \text{ eV} . \quad (87)$$

The kinetic energy of the shrunken orbit sphere is $-\frac{1}{2}V$ or $T = 54.35$ eV. The ground-state hydrogen atom has a net energy of −13.59 eV, and the final hydrogen atom has a net energy of −54.42 eV (the same as He^+), and $\Delta E = -40.83$ eV for the reaction

$$H(Z_{eff} = 1; r_1 = a_0) \rightarrow H(Z_{eff} = 2; r_{1/2} = 0.5a_0) . \quad (88)$$

That is, ~27 eV is lost with the absorption of the energy hole, and −14 eV is given off after absorption of the energy hole.

It is shown later that the resonance energy hole of a hydrogen atom that excites resonator modes of radial dimensions $a_0/(m+1)$ is

$$m \times 27.2 \text{ eV} , \quad (89)$$

where

$$m = 1,2,3,4,\ldots .$$

After resonant absorption of the hole, the radius a_0 of the orbit sphere shrinks to $a_0/(m+1)$, and after p cycles of resonant shrinkage, the radius is $a_0/(mp+1)$.

In other words, the radial ground-state field can be considered as the superimposition of Fourier components. The removal of negative Fourier components of energy $m \times 27.2$ eV, where m is an integer, gives rise to a larger positive electric field inside the spherical shell, which is a time-harmonic solution of Laplace's equations in spherical coordinates. In this case, the radius at which force balance and nonradiation are achieved is $a_0/(m+1)$, where m is an integer. In decaying to this radius from the ground state, a total energy of $[(m+1)^2 - 1^2] \times 13.6$ eV is released. The process is hereafter referred to as hydrogen emission by catalytic thermal electronic relaxation (HECTER).

The electric field of a hydrogen atom, or a deuterium atom, is zero for $r > r_n$, where r_n is the radius of the orbit sphere of the electron. Thus, as the orbit sphere shrinks, approaching nuclei experience a smaller Coulombic barrier, and the internuclear distance (between two deuterium atoms, for example) shrinks as well. As the internuclear separation decreases, fusion is more probable. In muon-catalyzed fusion, for example, the internuclear separation is reduced by ~200 (the muon-to-electron mass ratio), and the fusion rate increases by ~80 orders of magnitude. In a catalytic system that produces energy holes of 27.21 eV, deuterium atoms can be repeatedly shrunk, and the internuclear separation can be much smaller than the muon reduction. These smaller internuclear distances yield much higher fusion rates. Mills and Farrell[1] call this fusion process Coulombic annihilation fusion (CAF).

It is important to note that the products of CAF are tritium, ^3H, and protons, ^1H. In hot fusion, deuterium nuclei collide randomly and produce ~50% ^3H plus ^1H and ~50% ^3He plus a neutron. In CAF, however, the nuclei are moving slowly and will collide in the most favored Coulombic arrangement—with the two protons as far from each other as possible. Thus, for CAF, significantly more ^3H will be produced than ^3He.

Titanium(II) is one of the catalysts that can cause resonant shrinkage because the third ionization energy is 27.49 eV [$m = 1$ in Eq. (89)]. Thus, the shrinkage cascade for the p'th cycle is

$$27.491 \text{ eV} + Ti^{2+} + {}^2H\left(\frac{a_0}{p}\right) \rightarrow Ti^{3+} + e^- + {}^2H\left[\frac{a_0}{(p+1)}\right]$$

$$+ [(p+1)^2 - p^2] \times 13.6 \text{ eV} \quad (90)$$

and

$$Ti^{3+} + e^- \rightarrow Ti^{2+} + 27.491 \text{ eV} . \quad (91)$$

The overall reaction is

$${}^2H\left(\frac{a_0}{p}\right) \rightarrow {}^2H\left[\frac{a_0}{(p+1)}\right] + [(p+1)^2 - p^2] \times 13.6 \text{ eV} . \quad (92)$$

Note that the energy given off as the atom shrinks is much greater than the energy lost to the energy hole, and the energy released is large compared to conventional chemical reactions.

Rubidium(I) is also a potential catalyst. The second ionization energy is 27.28 eV:

$$27.28\text{ eV} + Rb^+ + {}^2H\left(\frac{a_0}{p}\right) \rightarrow Rb^{2+} + e^- + {}^2H\left[\frac{a_0}{(p+1)}\right] + [(p+1)^2 - p^2] \times 13.6\text{ eV} \quad (93)$$

and

$$Rb^{2+} + e^- \rightarrow Rb^+ + 27.28\text{ eV} . \quad (94)$$

The overall reaction is the same as Eq. (92).

Less efficient catalytic systems hinge on the coupling of three resonator cavities. For example, the third ionization energy of palladium is 32.93 eV. This energy hole is obviously too high for resonant absorption. However, Li(I) releases 5.392 eV when it is reduced to Li. The combination of Pd(II) to Pd(III) and Li(I) to Li, then, has a net energy change of 27.54 eV:

$$27.54\text{ eV} + Li^+ + Pd^{2+} + {}^2H\left(\frac{a_0}{p}\right) \rightarrow Li + Pd^{3+} + {}^2H\left[\frac{a_0}{(p+1)}\right] + [(p+1)^2 - n^2] \times 13.6\text{ eV} \quad (95)$$

and

$$Li + Pd^{3+} \rightarrow Li^+ + Pd^{2+} + 27.54\text{ eV} . \quad (96)$$

The overall reaction is the same as Eq. (92).

An efficient catalytic system that hinges on the coupling of three resonator cavities involves potassium. For example, the second ionization energy of potassium is 31.63 eV. This energy hole is obviously too high for resonant absorption. However, K(I) releases 4.34 eV when it is reduced to K. The combination of K(I) to K(II) and K(I) to K, then, has a net energy change of 27.28 eV.

$$27.28\text{ eV} + K^+ + K^+ + {}^2H\left(\frac{a_0}{p}\right) \rightarrow K + K^{2+} + {}^2H\left[\frac{a_0}{(p+1)}\right] + [(p+1)^2 - n^2] \times 13.6\text{ eV} \quad (97)$$

and

$$K + K^{2+} \rightarrow K^+ + K^+ + 27.28\text{ eV} . \quad (98)$$

The overall reaction is the same as Eq. (92).

In general, absorption of an energy hole causes the orbit sphere to undergo a transition from one stable nonradiative radius to another stable nonradiative radius. The Coulombic force is attractive; thus, the orbit sphere shrinks when the effective nuclear charge increases. The orbit sphere has an initial radius r_n, initial effective nuclear charge Z_{eff}, and initial velocity v_n given by the condition for nonradiation:

$$2\pi(nr_1) = n\lambda_1 , \quad n = 1, \frac{1}{2}, \frac{1}{3}, \frac{1}{4}, \ldots , \quad (99)$$

and

$$v_n = \frac{\hbar}{m_e n a_0} . \quad (100)$$

At force balance,

$$\frac{\hbar^2}{m_e (r_n)^3} = \frac{Z_{eff} e^2}{4\pi\epsilon_0 (r_n)^2} . \quad (101)$$

Shrinkage occurs because the effective nuclear charge increases by an integer m when Eqs. (99), (100), and (101) are satisfied by the introduction of an energy sink of a coupled resonator, such as an electron orbit sphere resonator cavity comprising an electrochemical couple. The coupled resonator provides energy holes and affects the shrinkage transition from the initial radius $a_0/(mp+1)$ and a nuclear charge of $(mp+1)$ to the second radius $\{a_0/[m(p+1)+1]\}$ and a nuclear charge of $m(p+1)+1$. Energy conservation and the boundary condition that trapped photons must be a solution to Laplace's equation determine that the energy hole to cause a shrinkage is given by Eq. (89). As a result of coupling, the deuterium atom emits a photon of $m \times 27.21$ eV, and this photon is absorbed by the coupled resonator. Stated another way, the deuterium atom absorbs an energy hole of $m \times 27.21$ eV. The energy hole absorption causes a second photon to be trapped in the deuterium atom electron orbit sphere. Recall from Sec. III that electromagnetic radiation of discrete energy can be trapped in a resonator cavity. As shown previously, the photonic equation must be a solution of Laplace's equation in spherical coordinates. The photon field comprises an electric field that provides force balance and a nonradiative orbit sphere. The solution to this boundary value problem of the radial photon electric field is given by

$$\epsilon \vec{i}_{r\,photon\,j,l,m} = \frac{e}{4\pi\epsilon_0} \frac{(na_0)^l}{r^{(l+2)}} \{-1 + n[Y_l^m(\phi,\theta) + Y_s^{m_s}]\} . \quad (102)$$

It is apparent from this equation that, for $l = 0$ and given an initial radius of $\{a_0/(mp+1)\}$ and a final radius of $\{a_0/[m(p+1)+1]\}$, the nuclear charge is increased by m with the absorption of an energy hole of $m \times 27.2$ eV. The potential energy decreases by this energy; thus, energy is conserved. However, the force balance equation is not initially satisfied as the effective nuclear charge increases by m. Further energy is emitted as force balance is achieved at the final radius. By replacing the initial radius with the final radius and by increasing the charge by m in Eq. (101),

$$[m(p+1)+1]^3 \frac{\hbar^2}{m_e a_0^3} = [m(p+1)+1]^2 \frac{\{[m(p+1)+1]e\}e}{4\pi\epsilon_0 a_0^2} , \quad (103)$$

force balance is achieved and the orbit sphere is nonradiative.

The energy balance for $m = 1$ is as follows. An initial energy of 27.21 eV is emitted as the energy hole absorption event. This increases the effective nuclear charge by one and decreases the potential by 27.21 eV. More energy is emitted until the total energy released is $[(p+1)^2 - p^2] \times 13.6$ eV.

In general, the resonance energy to cause shrinkage of the radius from a_0 to $a_0/(m+1)$ is $m \times 27.21$ eV, where $m = 1,2,3,4$. The resonant absorption of this energy hole causes the effective nuclear charge to increase by m. And, the energy released in going from infinity to $a_0/(m+1)$ is $(m+1) \times (m+1) \times 13.6$ eV or $(m+1)^2 \times 13.6$ eV.

Energy holes add. The corresponding effective charges resulting from the absorption of energy holes also add. Thus, any combination of energy holes that sums to $m \times 27.21$ eV,

where m is the same as the m for the final radius ($a_0/m + 1$) leads to shrinkage to the same final radius of the orbit sphere.

VI. METHODS

A search for excess heat during the electrolysis of aqueous potassium carbonate (K^+/K^+ electrocatalytic couple) was investigated using single-cell, silvered, vacuum-jacketed dewars. To simplify the calibration of these cells, they were constructed to have primarily conductive heat losses. Thus, a linear calibration curve was obtained. Three methods of differential calorimetry were used to determine the cell constant, which was used to calculate the excess enthalpy:

1. The cell constant was calculated during the experiment (on-the-fly-calibration) by turning an internal resistance heater off and on and inferring the cell constant from the difference between the losses with and without the heater.

2. The cell constant was determined with no electrolysis processes occurring by turning an internal resistance heater off and on for a well-stirred dewar cell and inferring the cell constant from the difference between the losses with and without the heater. This method overestimates the cell constant because there is no gas flow (which adds to the heat losses).

3. In the third method, rather than keeping the ambient temperature constant while raising the cell temperature with heater power input, the ambient temperature was lowered and heater power was applied to maintain a constant cell temperature. This method caused the least perturbation to temperature-dependent electrochemical processes.

The general form of the energy balance equation for the cell in steady state is

$$0 = P_{appl} + Q_{htr} + Q_{xs} - P_{gas} - Q_{loss} , \quad (104)$$

where

P_{appl} = electrolysis power

Q_{htr} = power input to the heater

Q_{xs} = excess heat power generated by an unknown process

P_{gas} = power removed as a result of evolution of H_2 and O_2 gases

Q_{loss} = thermal power loss from the cell.

When an aqueous solution is electrolyzed to liberate hydrogen and oxygen gases, the electrolysis power P_{appl} ($= E_{appl}I$) can be partitioned into two terms:

$$P_{appl} = E_{appl}I = P_{cell} + P_{gas} . \quad (105)$$

An expression for P_{gas} ($= E_{gas}I$) is readily obtained from the known enthalpy of formation of water from its elements:

$$E_{gas} = \frac{-\Delta H_{form}}{\alpha F} ,$$

where F is Faraday's constant, which yields $E_{gas} = 1.48$ V for the reaction

$$H_2O \rightarrow H_2 + \tfrac{1}{2}O_2 .$$

The net Faradaic efficiency of gas evolution is assumed to be unity; thus, Eq. (105) becomes

$$P_{cell} = (E_{appl} - 1.48V)I . \quad (106)$$

The cell was calibrated for heat losses by turning an internal resistance heater off and on while maintaining constant electrolysis and by inferring the cell conductive constant from the difference between the losses with and without the heater, where heat losses were primarily conductive losses through the top of the dewar. When the heater was off, the losses were given by

$$c(T_c - T_b) = P_{appl} + 0 + Q_{xs} - P_{gas} , \quad (107)$$

where

c = conductive heat loss coefficient

T_b = ambient temperature

T_c = cell temperature.

When a new steady state is established with the heater on, the losses change to

$$c(T'_c - T_b) = P'_{appl} + Q_{htr} + Q'_{xs} - P'_{gas} , \quad (108)$$

where a superscript prime indicates a changed value when the heater was on. When the following assumptions apply,

$$Q_{xs} = Q'_{xs} ,$$

$$P_{appl} = P'_{appl} ,$$

and

$$P_{gas} = P'_{gas} ,$$

the cell constant a, the reciprocal of the conductive loss coefficient c, is given by

$$a = \frac{T'_c - T_c}{Q_{htr}} . \quad (109)$$

Also, the slope of the plot of $\Delta T = T_c - T_B$ versus $P_T = Q_{htr} + P_{cell}$ is the cell constant:

$$a = \frac{\Delta T' - \Delta T}{\Delta P_T} . \quad (110)$$

VII. EXPERIMENTAL

An electrolytic cell was assembled comprising a 500-ml, silvered, vacuum-jacketed dewar with a 5-cm opening covered with a 0.75-in.-thick tapered rubber stopper (vessel A) fitting 0.25 in. into the dewar mouth or a 200-ml, silvered, vacuum-jacketed dewar with a 3-cm-diam opening covered with Parafilm (vessel B).

The cathode was a 7.5-cm-wide × 5-cm-long × 0.125-mm-thick nickel foil (Aldrich 99.9+%) spiral with a 9-mm diameter and 2-mm pitch with a nickel lead strip (cathode A) or a 5-cm-long × 0.75-cm-diam graphite rod with a 0.127-mm platinum lead (cathode B). The nickel cathode was prepared by tightly rolling the nickel foil about a 9-mm rod. The rod was removed, and the spiral was formed by partially unrolling the foil.

The anode was a 10-cm × 1-mm-diam spiraled platinum wire (Johnson-Matthey) with a 0.127-mm platinum lead wire (anode A) or a 2.5-cm-diam × 7.5-cm-high platinum basket with a 1-mm-diam platinum lead wire (anode B). When anode A was utilized, the cathode/anode separation distance was 1 cm. When anode B was used, the cathode/anode separation distance was 1.2 cm.

The electrolyte solution was 100 ml of 0.57 M aqueous K_2CO_3 (Aldrich $K_2CO_3 * \frac{3}{2}H_2O$ 99+%) (solution A) or

100 ml of 0.57 *M* aqueous Na_2CO_3 (Aldrich Na_2CO_3 American Chemical Society primary standard 99.95+%) (solution B).

The resistance heater used during calibration and operation comprised a 100 or 10.5 Ω, 1% precision metal oxide resistor in a 2-mm-o.d. Teflon tubing powered by a variable direct current (dc) voltage power source (±0.5%).

A constant dc current (±0.1%) was provided by the circuit shown in Fig. 1 (mode C). A constant dc voltage power supply (±0.5%) was used directly in the continuous current mode (mode B). A power controller with the circuit shown in Fig. 2 was used to provide intermittent current (mode A). The current voltage parameters were an intermittent square-wave with an offset voltage of −2.2 V, a peak voltage of −2.75 V, a peak current of −175 mA, an −35% duty cycle, and a frequency of −500 Hz. The voltage and current waveforms are shown in Figs. 3 and 4, respectively.

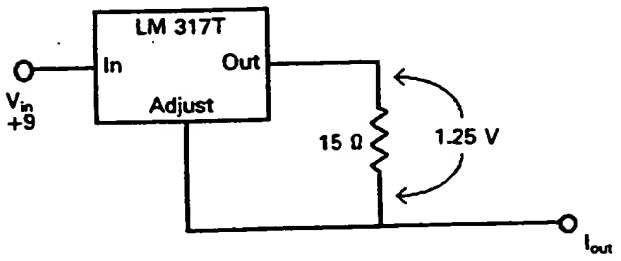

Fig. 1. Schematic of the circuit used to provide constant dc current.

In stirring mode A, the electrolyte solution was stirred with a 7-mm × 2-cm spheroidal ellipse magnetic stirring bar that was spun by a 6-cm-long open magnet mounted on an open shaft revolving at 750 rpm under the dewar. The shaft was that of an open mixing motor (Flexa-Mix model 76, Fisher). The temperature correction for the Joule heating of stirring was determined from an identical experimental apparatus that was only stirred.

In stirring mode B, the electrolyte solution was stirred by a 2-cm-wide × 1-cm-high glass paddle connected to a 40-cm-long × 5-mm-o.d. glass rod that entered the dewar vertically through a 6-mm-i.d. vacuum greased glass tube implanted through the rubber stopper covering the dewar. The rod was rotated at 380 rpm by a mixing motor (Lightnin model L, Mixing Equipment Company) controlled by a variable autotransformer (Powerstat model 116B). The temperature correction for the Joule heating of stirring was determined by stirring the electrolyte and measuring its temperature relative to the temperature of an unstirred matched cell before initiating an experiment. Otherwise, the experiments were stirred by gas sparging from the gases produced during electrolysis.

Nickel cathodes were initially operated in reverse polarity with a continuous or time-averaged current of 80 mA for 30 min to break in a new cathode. This operation conditions the electrode and makes the electrolysis more surface uniform. Following any change in heater power, an intentional ambient temperature change, or commencement of electrolysis, time was allowed for the cell temperature to establish a

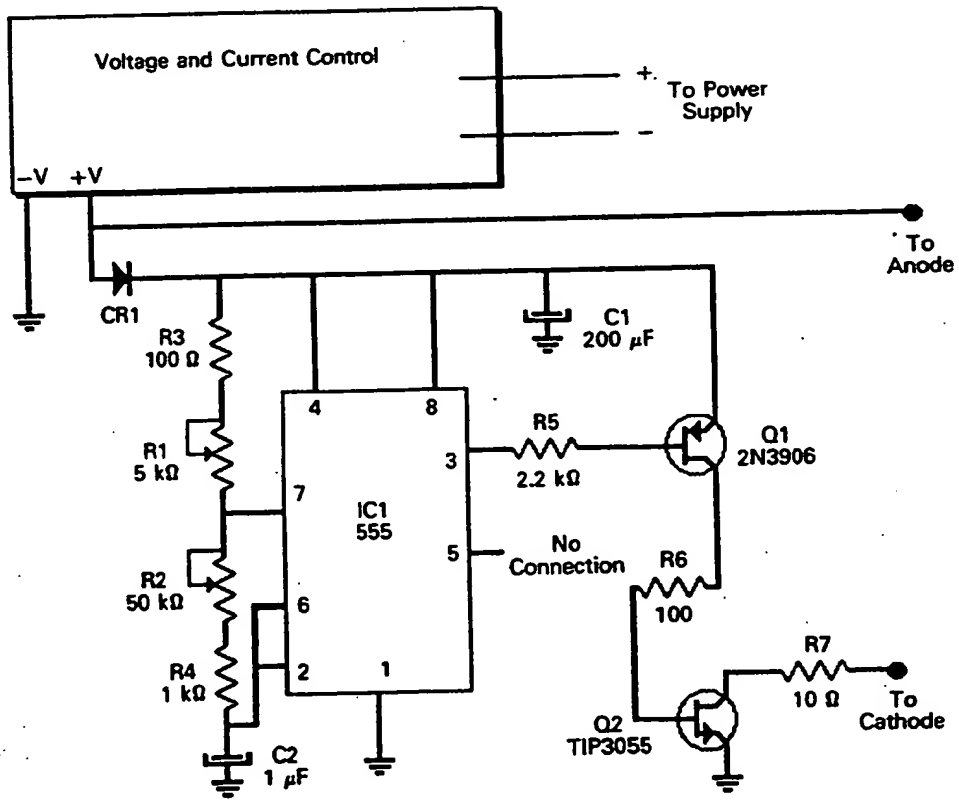

Fig. 2. Schematic of the circuit used to provide intermittent (on/off) dc voltage.

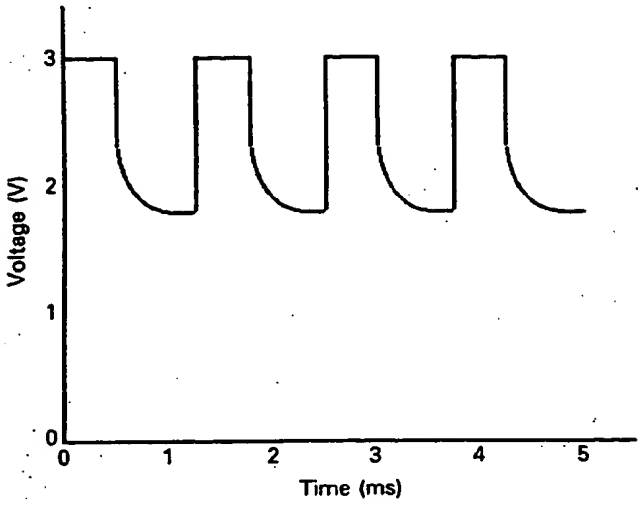

Fig. 3. Voltage versus time oscilloscope trace of the circuit of Fig. 2.

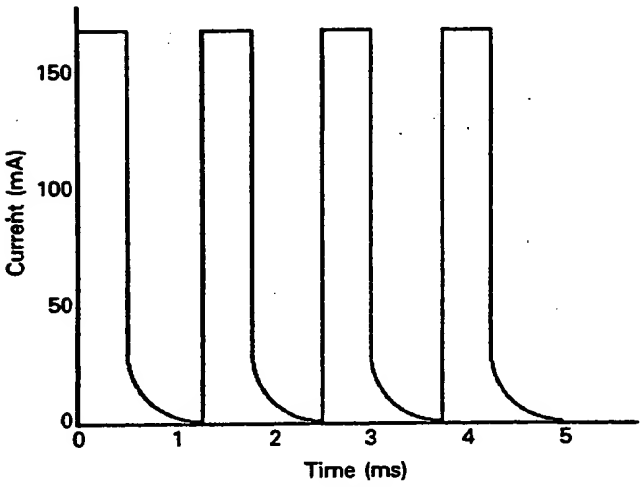

Fig. 4. The current versus time oscilloscope trace of the circuit of Fig. 2.

new steady state before data were recorded. The time for the temperature to stabilize following the commencement of electrolysis was typically 12 h. The time for the temperature to stabilize following an increase of heater power of ~0.3 W was ~4 h for cells with no electrolysis and for electrolytic cells operating for >12 h. The dewar was agitated prior to a temperature reading to ensure thorough thermal mixing.

The outside of the vessel was maintained at ambient air temperature, which was monitored, and the difference between cell and a matched nonoperative cell was determined with a thermometer (±0.1°C). Ambient temperature fluctuations per 24 h were typically <0.5°C. (The matched nonoperative cell was structurally and chemically identical, but the electrolysis current was zero and the heater power was zero. In the case of stirring mode A, the matched nonoperative cell was stirred identically.)

For another method, rather than keeping the ambient temperature constant while raising the cell temperature with heater power input, the ambient temperature was lowered by adjusting the thermostatic control of the room temperature, and heater power was applied to maintain an approximately constant cell temperature. The room temperature and heater power were adjusted until the excess heat before and after the change in ambient temperature were equal. The ambient temperature reached a steady-state temperature (±0.1°C) in 8 h, and the cell reached a steady-state temperature (±0.1°C) 4 h later. The temperature difference between the cell and a matched nonoperative cell was determined with a thermometer (±0.1°C).

For circuit A, peak voltage measurements were made with an oscilloscope (BK model 2120), and the time-averaged current was determined from a multimeter voltage measurement (±0.2%) across a calibrated resistor (1 Ω) in series with the lead to the cathode. The waveform of the pulsed cell was a square wave. Since there was current only during the peak voltage interval of the cycle, P_{appl} [Eq. (105)] is given by the product of the peak voltage and the peak current and the duty cycle, which is the product of the peak voltage and the time-averaged current. In circuit B, voltage across the cell was measured with the multimeter, and the current was determined from the multimeter voltage measurement across a calibrated resistor (1 Ω) in series with the lead to the cathode. For this mode, P_{appl} [Eq. (105)] is given by the product of the constant voltage and the constant current.

VIII. RESULTS

A summary of the results of the excess enthalpy released during the electrolysis of potassium carbonate (K^+/K^+ electrocatalytic couple) as well as the results for the control (sodium carbonate, for which no electrocatalytic reaction of −27.21 eV is possible) are given in Table I, which also lists the experiment number. Experiments designated with a number followed by an "A" had heat added to the experiment designated by the same number.

Figures 5 through 9 show the difference between experimental cell temperature and the temperature of a matched

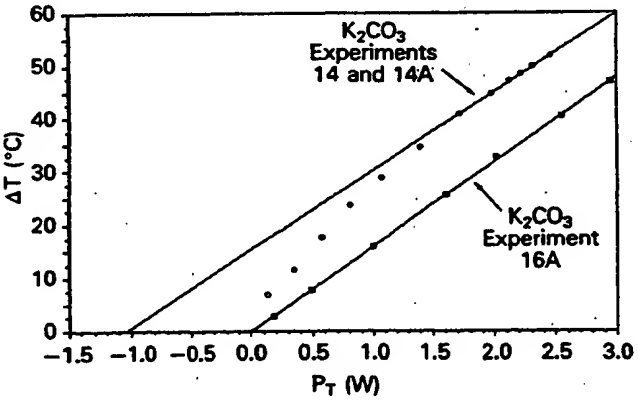

Fig. 5. Plots of the differences between cell temperature and the temperature of a matched nonoperative cell (ΔT) as a function of total power P_T for (a) K_2CO_3 experiments 14 and 14A in which the electrolysis current was maintained at −85 mA and (b) K_2CO_3 experiment 16A in which electrolysis current was zero. Increasing temperatures were recorded as the calibration resistor was stepped in power. The curves are fit to the solid symbols.

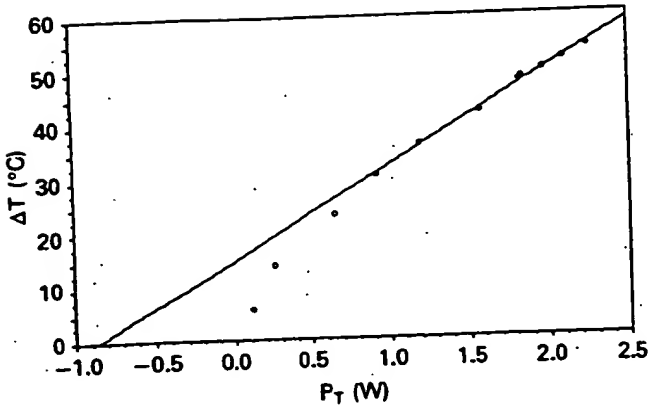

Fig. 6. Plot of the difference between cell temperature and the temperature of a matched nonoperative cell (ΔT) as a function of total power P_T for K_2CO_3 experiments 15 and 15A, in which the electrolysis current was maintained at 82 mA. Increasing temperatures were recorded as the calibration resistor was stepped in power. The curve was fit to the solid circles.

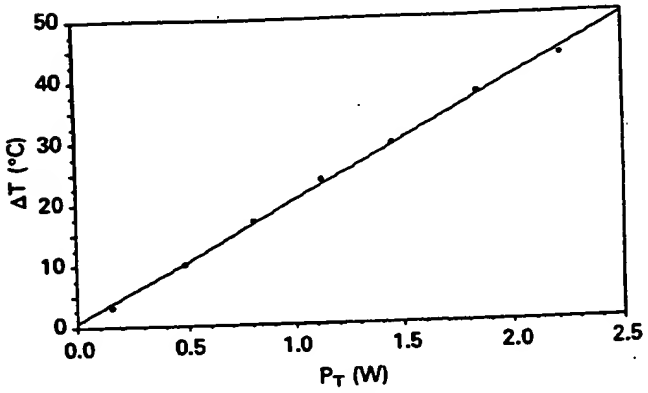

Fig. 7. Plot of the difference between cell temperature and the temperature of a matched nonoperative cell (ΔT) as a function of total power P_T for K_2CO_3 experiment 17A. The electrolysis current was zero. Increasing temperatures were recorded as the calibration resistor was stepped in power.

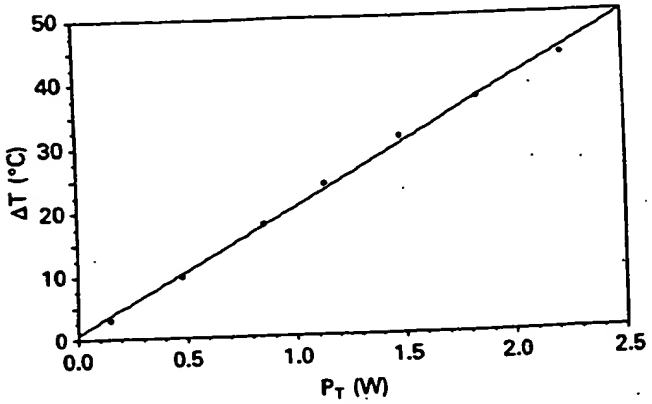

Fig. 8. Plot of the difference between cell temperature and the temperature of a matched nonoperative cell (ΔT) as a function of total power P_T for Na_2CO_3 experiments 18 and 18A. The electrolysis current was maintained at 79.7 mA. Increasing temperatures were recorded as the calibration resistor was stepped in power.

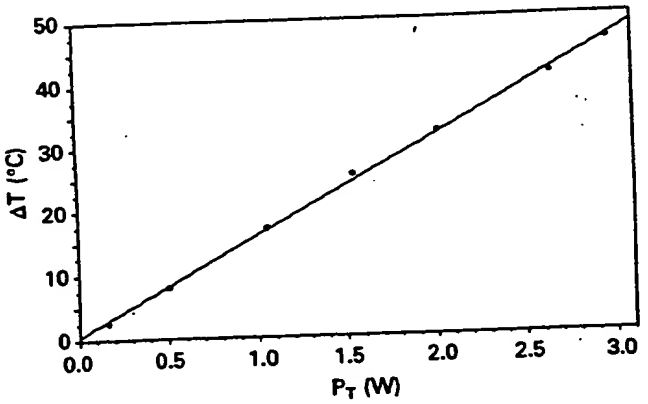

Fig. 9. Plot of the difference between cell temperature and the temperature of a matched nonoperative cell (ΔT) as a function of total power P_T for Na_2CO_3 experiments 19 and 19A. The electrolysis current was maintained at 79.7 mA. Increasing temperatures were recorded as the calibration resistor was stepped in power.

nonoperative cell (ΔT) as a function of total power P_T for different electrolysis currents. The value of P_T is

$$P_T = P_{cell} + Q_{htr} ,$$

where P_{cell} is calculated using Eq. (106). Increasing temperatures were recorded as the calibration resistor was stepped in power.

In K_2CO_3 experiment 16A, there was no hydrogen to react, and this experiment is a control of differential calorimetry for K_2CO_3 experiments 14 and 14A. The plot for K_2CO_3 experiment 16A (see Fig. 5) is linear with an x intercept and a y intercept of zero, which indicates no excess heat. However, the plot for K_2CO_3 experiments 14 and 14A (K^+/K^+ electrocatalytic couple) (see Fig. 5) is highly nonlinear in the 25 to 50°C temperature range and approximately linear thereafter. Interpolation of the linear data to the y intercept indicates an excess temperature of ~15°C. Interpolation of the linear data to the x intercept indicates an excess power of ~10 times the input power.

The plot of ΔT versus P_T for Na_2CO_3 experiments 18 and 18A and 19 and 19A are shown in Figs. 8 and 9, respectively. No electrocatalytic reaction of ~27.21 eV is possible for sodium; thus, these experiments represent controls that are essentially chemically identical but lack an electrocatalytic couple to induce the electrons of hydrogen atoms to relax to a quantized potential energy level below that of the ground state by providing a redox energy-energy hole (27.28 eV) resonant with this transition. These plots are linear with an x intercept and a y intercept of zero, which indicates no excess heat. However, the plots for K_2CO_3 experiments 14, 14A, 15, and 15A (K^+/K^+ electrocatalytic couple), shown in Figs. 5 and 6, respectively, are highly nonlinear in the 25 to 50°C

TABLE

Percentage Excess Enthalpy Where the Cell Constant

Experiment	Solution	Cathode	Anode	Vessel	Stirring Mode	Mode	Duty Cycle (%)	Frequency (Hz)
K_2CO_3								
1	A	A	A	A		A	40	500
1A	A	A	A	A		A	40	500
1AA	A	A	A	A		A	40	500
2	A	A	A	A		A	35	500
2A	A	A	A	A		A	35	500
3	A	B	A	A		A	40	500
3A	A	B	A	A		A	35	500
4	A	A	A	A		A	35	500
4A	A	A	A	A		A	35	500
5	A	A	A	A		A	35	500
5A	A	A	A	A		A	35	500
6	A	A	A	A		A	35	500
6A	A	A	A	A		A	35	500
7	A	A	A	A		A	35	500
7A	A	A	A	A		A	35	500
8	A	A	A	A		B		
8A	A	A	A	A		B		
9	A	A	A	A		A	35	500
9A	A	A	A	A		A	35	500
10	A	A	A	A		A	35	500
10A	A	A	A	A		A	35	500
11A	A	A	A	A		A	35	500
12A	A	A	A	A	A	B		
13	A	A	A	A		A	35	500
13A	A	A	A	A		A	35	500
14	A	A	A	A	B	B		
14A	A	A	A	A	B	B		
15	A	A	B	B		C		
15A	A	A	B	B		C		
16A	A	A	A	A	A			
17A	A	A	A	A	A			
Na_2CO_3								
18	B	A	A	A	A	C		
19	B	A	A	A	A	C		

*See Sec. VII for an explanation of the experimental configurations.
[a]Q_{htr} = heater watts added to raise the temperature of the cell during operation.
[b]$\Delta T = T_c - T_b$.
[c]$\Delta T_{htr} = aQ_{htr}$ = temperature change in the cell due to the heater.
[d]$\Delta\Delta T = \Delta T - \Delta T_{htr}$.
[e]$\Delta T_{cell} = aP_{cell}$.

temperature range and approximately linear thereafter. Interpolation of the linear data to the y intercept indicates an excess temperature of ~15°C. Interpolation of the linear data to the x intercept indicates an excess power of ~10 times the input power. For each experiment, the upper limit of the cell parameter a was determined from the slope at ~55°C.

Linear plots of ΔT versus P_T for heater alone (no electrolysis) K_2CO_3 control experiments 16A (Fig. 5) and 17A (Fig. 7), which go through zero at the origin, validate the original assumptions that the losses were conductive. The upper limit of the cell parameter a was determined from the slope. The cell parameter was slightly lower for electrolytic cells compared to matched nonelectrolytic cells, as shown in Fig. 5. This is attributed to the additional heat loss due to gas flow in the electrolytic cells.

The results of the determination of the cell constant, Q_{xs}, and Q'_{xs} at an operating temperature of ~32°C appear in Table II. For calibration runs (K_2CO_3 experiments 20A1, 20A2, 20A3, and 20A4), the ambient temperature was ~2 to 5°C lower than in the reference cell (K_2CO_3 experiment 20),

I

Was Determined by On-the-Fly-Calibration*

Offset Voltage (V)	Peak Voltage (V)	Peak Current (mA)	Cell Constant (°C/W)	Q_{htr}[a] (W)	ΔT[b] (°C)	ΔT_{htr}[c] (°C)	$\Delta\Delta T$[d] (°C)	ΔT_{cell}[e] (°C)	Excess Heat[f] (%)
								2.08	328
2.73	3.43	180	14.8	0	8.9			1	1234
2.36	2.96	112	15	1.044	29	15.67	13.33	2.17	557
2.32	3.22	212	14.8	2.196	47.2	32.9	14.3	1.56	169
2.19	2.79	231	14.8	0	4.2			1.88	544
2.55	3.15	217	14.8	2.196	45	32.9	12.1		
								2.42	156
2.93	3.63	163	14.8	0	6.2			2.17	662
2.795	3.295	231	14.8	2.196	49.5	32.94	16.56	1.58	183
2.185	2.685	254	14.8	0	4.5			1.19	1016
2.02	2.42	245	14.8	2.21	46.5	33.17	13.33	1.45	231
2.12	2.72	225	14.8	0	4.8				
								1.32	634
2.01	2.51	248	14.8	2.22	43	33.3	9.7	1.71	215
2.425	3.125	205	14.5	0	5.4			1.57	612
2.47	2.97	208	14.5	2.22	44.5	33.3	11.2	1.74	147
2.17	2.77	246	15.7	0	4.3			1.33	705
2.04	2.54	228	15.7	0.911	25	14.3	10.7		
								1.19	252
	2.42	75	16.9	0	4.2			1.08	953
	2.28	80	16.9	0.99	28.1	16.73	11.37	0.626	395
2.1	2.4	131	14.8	0	3.1			0.367	3766
2	2.1	114	14.8	0.778	25.7	11.51	14.19	0.551	408
2.1	2.4	117	14.6	0	2.8				
								0.461	2621
2	2.25	117	14.6	1.96	41.2	28.65	12.5	0.95	838
2.5	2.8	114	18	0.76	22.6	13.68	8.91	1.036	1027
	2.31	80	15.6	0.771	23.7	12	11.7	1.39	217
2	2.55	243	15.25	0	4.4			1.3	1094
2.1	2.6	217	15.25	1.537	38.9	23.4	15.5		
								2.01	243
	3.08	85	14.8	0	6.9			1.87	830
	2.9	89	14.8	1.59	40.9	23.5	17.4	1.82	213
	2.748	82	17.5	0	5.7			1.01	1355
	2.247	82	17.5	2.028	51.5	35.5	16.01		
			15.9						
			15.5						
								3.14	1.9
	3.48	79.7	19.7	0	3.2			2.95	1.6
	3.37	79.7	19.6	0	3				

[f]Excess heat = $\begin{cases} \dfrac{\Delta T - \Delta T_{cell}}{\Delta T_{cell}} \times 100\,, & \text{when heater was off} \\ \dfrac{\Delta\Delta T - \Delta T_{cell}}{\Delta T_{cell}} \times 100\,, & \text{when heater was on} \end{cases}$

and heater power was added to make the temperature of each calibration cell approximately equal to the cell temperature of the reference cell. The cell constant was determined by subtracting Eq. (107) with the parameters of the reference run from Eq. (108) with the parameters of each calibration run, and Eq. (106) was used to determine P_{cell} for each equation. It was assumed that the losses were conductive and that $Q_{ss} = Q'_{ss}$. The assumption that the losses Q_{loss} were conductive for these silvered dewars is supported by the data of Figs. 8 and 9. The assumption that $Q_{ss} = Q'_{ss}$ was verified by calculating these parameters from the cell constant determined.

IX. DISCUSSION

The data clearly indicate that excess heat was generated. Once the technique was perfected, each experiment using potassium carbonate produced excess heat. Some experiments were permitted to operate for weeks, and the excess heat remained relatively constant. What is the source of this excess

TABLE

Determination of the Cell Constant by Lowering the Ambient Temperature

Experiment	Solution	Cathode	Anode	Vessel	Stirring Mode	Mode	Voltage (V)
K_2CO_3							
20	A	A	A	A	B	B	2.38
20A1	A	A	A	A	B	B	3.08
20A2	A	A	A	A	B	B	3.11
20A3	A	A	A	A	B	B	3.11
20A4	A	A	A	A	B	B	3.2

enthalpy? Electrochemical reactions that consume the electrolyte can be ruled out because any proposed electrochemical reactant would be completely consumed over the duration of these experiments. Nickel forms a hydride during cathodic electrolysis, but this process is endothermic.[6] The weight of the nickel cathode was unchanged by use in a heat-producing cell to within 0.00001 g (the cathode was rinsed after 36 h of operation, then dried and degassed in vacuum before the final weight was determined). The only remaining candidates are heat-releasing reactions involving the electrolytically generated hydrogen or oxygen atoms or molecules. Because the excess enthalpy exceeds that which can be accounted for due to complete recombination, new processes must be sought.

The results are consistent with the release of heat energy from hydrogen atoms where the K^+/K^+ electrocatalytic couple induces the electrons of hydrogen atoms to relax to a quantized potential energy level below that of the ground state by providing a redox energy-energy hole (27.28 eV) resonant with this transition. The balanced reaction is given by Eqs. (92), (97), and (98). Excess heat was also measured when K_2CO_3 was replaced by Rb_2CO_3. The Rb^+ ion (energy hole from the second ionization is 27.28 eV) alone is electrocatalytic according to the reaction given by Eqs. (92), (93), and (94). No excess heat was observed when K_2CO_3 was replaced by Na_2CO_3 as demonstrated with Na_2CO_3 experiments 18 and 18A and 19 and 19A, shown in Figs. 8 and 9, respectively. For sodium or sodium ions, no electrocatalytic reaction of -27.21 eV is possible. For example, 42.15 eV of energy is absorbed by the reverse of the reaction given in Eq. (98), where Na^+ replaces K^+:

$$Na^+ + Na^+ + 42.15\ eV \rightarrow Na + Na^{2+} \ .$$

It has not been overlooked that other researchers have reported anomalous heat,[7] tritium,[7,8] and neutron production[7] during electrolysis of heavy water using a lithium salt electrolyte and a palladium cathode. The excess enthalpy is reported to be substantially larger than can be accounted for by nuclear reactions that produce tritium or neutrons.[7] In these cases, the couple is Pd^{2+}/Li^+ (27.54 eV). The balanced reaction is given by Eqs. (92), (95), and (96). The excess heat arises from the HECTER process, and the trace nuclear reactions are due to CAF as described in Sec. V. The HECTER process produces much greater quantities of heat energy than typical chemical reactions.

Neutron[9,10] and tritium[10] emissions from heavy water electrolytic cells using a titanium cathode and deuterium gas cells with titanium shavings have been reported. The tritium-to-neutron ratio is reported to be 10^8 (Ref. 10) as opposed to the 1:1 branching ratio of ^3H to ^3He observed for hot fusion. This result is anticipated for CAF. In the case of titanium, Ti^{2+} (27.49 eV) is electrocatalytic according to the reaction given by Eqs. (90), (91), and (92).

The data indicate that the shrinkage reaction is temperature dependent. This is clearly demonstrated by the nonlinear curves in Figs. 5 and 6 and by comparing the heated experiments (Table I) and the experiment of the same number for which heater power was zero. Most chemical reactions double their rates for each 10°C rise in temperature. Increasing temperature increases the collision rate between the hydrogen atoms and the electrocatalytic couple, which increases the shrinkage reaction rate. With large temperature excursions from room temperature, the kinetic energy distribution of the reactants can be sufficiently altered to cause the energy effecting the hydrogen shrinkage transition and the electrocatalytic redox reaction to conform to a greater or lesser extent. The rate is proportional to the extent of conformation or resonance of these energies.

The source of reactant hydrogen atoms is aqueous electrolytic production on the surface of the nickel cathode. Electrolysis and the associated ohmic losses consume (i.e., require) input power. The losses obviously rise with a rise in current. However, increased current increases the concentration of reactant hydrogen atoms. A trade-off exists between total excess power and percentage excess power. It was found that increasing the current with a concomitant increase in the concentration of reactant hydrogen atoms increases the total excess power but decreases the percentage excess power. During continuous electrolysis, much of the reactant hydrogen is lost as evolved gas. It was anticipated that more efficient production of reactant hydrogen could be provided by an electrolysis circuit that periodically generates reactant hydrogen atoms and allows them to react in the absence of further power dissipation. Comparing the experiments of Table I with pulsed peak current of -115 mA with those with continuous -80-mA current electrolysis, it can be appreciated that the efficiency of heat generation is correlated with the efficiency of hydrogen atom generation. For example, the input power of K_2CO_3 experiment 9A, which was pulsed, is one-third that of K_2CO_3 experiment 8A, which was operated with continuous current. The ratio of the percentage excess power of K_2CO_3 experiment 9A to K_2CO_3 experiment 8A is 3. An intermittent current (i.e., on-off) electrolysis circuit increases the percentage of excess heat by providing an optimal concentration of hydrogen atoms (reactants) while minimizing ohmic and electrolysis power losses. The frequency, duty cycle, peak voltage, step waveform, peak current, and offset voltage were adjusted to achieve the optimal shrinkage reaction rate and concomitant power while minimizing ohmic and

II

While Maintaining Constant Cell Temperature by Addition of Heat

Current (mA)	P_{cell} (W)	Q_{htr} (W)	P_T (W)	ΔT (°C)	Cell Constant	Q_{xs} (W)	Q'_{xs} (W)
79	0.0711	0	0.0711	3.2			
90	0.144	0.3249	0.4689	9.6	16.09	0.128	0.128
85	0.1386	0.1681	0.3067	7	16.13	0.127	0.127
81	0.132	0.2621	0.3942	8.4	16.095	0.128	0.128
100	0.172	0.2621	0.4341	9	15.98	0.129	0.129

electrolysis power losses. When the K^+/K^+ electrocatalytic couple was used with carbonate as the counterion, nickel as the cathode, and platinum as the anode, an intermittent square-wave with an offset voltage of ~2.2 V, a peak voltage of ~2.75 V, a peak current of ~120 mA, an ~35% duty cycle, and a frequency of ~500 Hz optimized the percentage excess power.

Although only the results for carbonate are reported, a strong dependence of the excess enthalpy on the structure and charge of the counterion was found. For carbonate, the transition state to the fractional quantized state of the hydrogen atom likely involves a neutral complex of carbonate with two juxtaposed potassium ions. The counterion of the electrocatalytic couple of the electrolytic solution can affect the shrinkage reaction rate by altering the energy of the transition state. For example, the transition state complex of the K^+/K^+ electrocatalytic couple with the hydrogen atom has a +2 charge and involves a three-body collision, which is unfavorable. A −2 charged oxyanion can bind the two potassium ions; thus, it provides a neutral transition-state complex of lower energy, whose formation depends on a binary collision, which is greatly favored. The rate depends on the separation distance of the potassium ions as part of the complex with the oxyanion. The greater the separation distance, the less favorable is the transfer of an electron between them. A close juxtaposition of the potassium ions increases the rate.

Further work to enhance the power, to search for chemical species with shrunken hydrogen atoms, and to search for products of predicted subsequent nuclear processes (CAF) following the shrinkage reaction are in progress. Preliminary data indicate that the electrolysis of a heavy water potassium carbonate electrolyte at a nickel cathode produces significant quantities of tritium, but the amount is much less than can account for the heat observed.

REFERENCES

1. R. L. MILLS and J. J. FARRELL, *The Grand Unified Theory*, Science Press (1989).

2. H. A. HAUS, "On the Radiation from Point Charges," *Am. J. Phys.*, 54, 1126 (1986).

3. D. A. McQUARRIE, *Quantum Chemistry*, University Science Books, Mill Valley, California (1983).

4. E. M. PURCELL, *Electricity and Magnetism*, McGraw-Hill Book Company, New York (1965).

5. I. S. HUGHES, *Elementary Particles*, Cambridge University Press (1972).

6. G. ALEFELD and J. VOLKL, Eds., *Hydrogen in Metals II*, p. 176, Springer Verlag (1967).

7. M. FLEISCHMANN, S. PONS, W. ANDERSON, L. J. LI, and M. HAWKINGS, "Calorimetry of the Palladium-Deuterium-Heavy Water System," *J. Electroanal. Chem.*, 287, 293 (1990).

8. E. STORMS and C. TALCOTT, in *Proc. Workshop on Cold Fusion Phenomena*, Santa Fe, New Mexico, May 23–25, 1989.

9. S. JONES et al., "Observation of Cold Nuclear Fusion in Condensed Matter," *Nature*, 338, 737 (1989).

10. P. IYENGAR et al., "Bhabha Atomic Research Centre Studies on Cold Fusion," *Fusion Technol.*, 18, 32 (1990).